ARMY RESEARCH LABORATORY

Long-Wave Infrared (LWIR) Polarimetric and Radiometric Analysis for a Variety of Thermal and Electromagnetic Suppressing Materials

by Kristan P Gurton and Scotlund McIntosh

ARL-TR-7009 **August 2014**

NOTICES

Disclaimers

The findings in this report are not to be construed as an official Department of the Army position unless so designated by other authorized documents.

Citation of manufacturer's or trade names does not constitute an official endorsement or approval of the use thereof.

Destroy this report when it is no longer needed. Do not return it to the originator.

Army Research Laboratory
Adelphi, MD 20783-1138

ARL-TR-7009 **August 2014**

Long-Wave Infrared (LWIR) Polarimetric and Radiometric Analysis for a Variety of Thermal and Electromagnetic Suppressing Materials

Kristan P Gurton
Computational and Information Sciences Directorate, ARL

Scotlund McIntosh
US Army Natick Soldier RDEC

REPORT DOCUMENTATION PAGE

Form Approved
OMB No. 0704-0188

1. REPORT DATE *(DD-MM-YYYY)*	2. REPORT TYPE	3. DATES COVERED (From - To)
August 2014	Final	January 2014

4. TITLE AND SUBTITLE
Long-Wave Infrared (LWIR) Polarimetric and Radiometric Analysis for a Variety of Thermal and Electromagnetic Suppressing Materials

5a. CONTRACT NUMBER

5b. GRANT NUMBER

5c. PROGRAM ELEMENT NUMBER

6. AUTHOR(S)
Kristan P Gurton and Scotlund McIntosh

5d. PROJECT NUMBER

5e. TASK NUMBER

5f. WORK UNIT NUMBER

7. PERFORMING ORGANIZATION NAME(S) AND ADDRESS(ES)
US Army Research Laboratory
ATTN: RDRL-CIE-S
2800 Powder Mill Road
Adelphi, MD 20783-1138

8. PERFORMING ORGANIZATION REPORT NUMBER
ARL-TR-7009

9. SPONSORING/MONITORING AGENCY NAME(S) AND ADDRESS(ES)

10. SPONSOR/MONITOR'S ACRONYM(S)

11. SPONSOR/MONITOR'S REPORT NUMBER(S)

12. DISTRIBUTION/AVAILABILITY STATEMENT
Approved for public release; distribution unlimited.

13. SUPPLEMENTARY NOTES

14. ABSTRACT

This technical report examines the polarimetric and radiometric properties of novel textile materials designed to suppress either thermal emission typically radiated by warm objects or attenuated stray electromagnetic (EM) fields that may damage electrical equipment, i.e., electromagnetic interference (EMI) shielding materials. Nine materials were examined: 3 forms of aluminum-coated heat-shield fabric, 2 samples of a nickel-Kevlar material, 2 samples of a silver-copper coated polyester material, and 2 weaves of a carbon-based textile material. Various-sized swaths of each material were placed on a temperature-controlled, black anodized-aluminum plate that was capable of tilting from 0° to 90°, where the angle is defined by the surface normal and the line of sight (LOS) of the sensor. Test-plate surface temperatures were intentionally kept moderate and ranged from 50 to 60 °C. Calibrated radiometric and polarimetric images were recorded at various orientations over a 5-day period in which the following parameters were measured for each material: the raw radiometric emission, S0 (w/sr-cm^2); the percentage of overall thermal radiance that was suppressed; the normalized Stokes parameters (S1 and S2); and the degree of linear polarization (DoLP). All parameters were determined in the long-wave infrared (LWIR) spectral region defined as 7.5–11.1 μm.

15. SUBJECT TERMS
Polarimetric imaging, LWIR

16. SECURITY CLASSIFICATION OF:			17. LIMITATION OF ABSTRACT	18. NUMBER OF PAGES	19a. NAME OF RESPONSIBLE PERSON
a. REPORT	b. ABSTRACT	c. THIS PAGE			Kristan P Gurton
Unclassified	Unclassified	Unclassified	UU	29	19b. TELEPHONE NUMBER (*Include area code*) 301-394-2093

Standard Form 298 (Rev. 8/98)
Prescribed by ANSI Std. Z39.18

Contents

List of Figures

1. Introduction

A polarimetric image is a two-dimensional representation in which each value in the array is a direct measure of the polarization state of the image-forming light that is captured by a polarimetric camera. This novel imaging methodology has been explored to varying degrees where the primary mode of operation was limited to the visible or near-infrared (NIR) regions of the electromagnetic (EM) spectrum.[1–4] However, there have been recent scientific studies designed to investigate the polarized nature of thermal emission in both the long-wave infrared (LWIR) and midwave infrared (MidIR) regions.[5–8]

Polarimetric sensors that operate in the thermal IR are designed to capture and analyze the polarization state of image-forming radiance emitted from warm objects and/or surfaces. It is well known that "man-made" objects emit thermal radiation that tends to have a preferential linear-polarization state, while naturally occurring "background" materials (vegetation, grass, trees, etc.) tend to show little or no preferential linear polarization. As a result, a thermal-polarimetric image can significantly enhance the ability to detect certain targets by increasing the contrast between man-made objects and their respective backgrounds, while simultaneously suppressing irrelevant clutter. Examples of Department of Defense (DOD)-related applications in which thermal-polarimetric imaging has been applied include the detection of disturbed earth associated with buried land mines and/or improvised explosive devices (IEDs), enhanced targeting and tracking of vehicles and personnel, and the identification of decoy objects.[9–12]

For this study we use the Stokes parameter method to describe the polarization state of the radiation that is emitted and/or reflected from a target area.[13] In order to define the polarization state of any EM wave, one measures the 4 Stokes parameters, S0, S1, S2, and S3, where S0 is related to the overall radiance intensity, S1 and S2 are measures of the degree of linear polarization, and S3 is a measure of how much of the light is circularly polarized. However, in practice the authors have never detected any form of circularly polarized radiance in the field and as a result we only consider the Stokes images S0, S1, and S2. The usual Stokes convention is followed where S1, S2, and S0 are defined as Equations 1–3:

$$S1 = I(0) - I(90) \ \ (w/sr\text{-}cm^2) , \tag{1}$$

$$S2 = I(+45) - I(-45) \ (w/sr\text{-}cm^2) . \tag{2}$$

For total linear polarization, the total radiance image, S0, is defined as

$$S0 = \text{total radiance} \ (w/sr\text{-}cm^2) , \tag{3}$$

and the degree-of-linear polarization (DoLP) image is expressed as

$$\text{DoLP} = \frac{\sqrt{S1^2 + S2^2}}{S0}, \tag{4}$$

where I(0), I(90), I(+45), and I(–45) represent captured imagery produced by polarized-radiance orientation angles 0°, 90°, +45°, and –45°, respectively, where 0° is defined as the vertical with respect to the image plane. As shown in Eqs. 1–3, the S1 image represents a relative measure of the vertical compared to the horizontal component, the S2 image represents a relative measure of the difference between the two ±45° diagonal states, and the S0 image is merely a conventional "intensity only" image. Finally, for this study, all values presented for the Stokes parameters are normalized with respect to the radiance image S0.

Figures 1a–1d show an example of a raw (unprocessed) polarimetric image set. The polarimetric images are of a vehicle at ambient temperature parked behind natural background. Figure 1a shows the conventional LWIR thermal image, S0, in which the pixel values are in radiance units of (w/sr-cm^2). Figure 1b shows the normalized S1 Stokes image, resulting in a pixel-value range of $-1 \leq S1 \leq 1$, where a negative S1 value signifies that the radiance is preferentially polarized in the horizontal plane and, conversely, positive S1 values represent preferential polarization in the vertical plane. Similarly, Fig. 1c and 1d show the normalized S2 and the corresponding DoLP-image product.

It should be noted that only a small degree-of-linear-polarization, e.g., 2–5%, is sufficient to generate good contrast for objects imaged against a natural background in which the DoLP typically is on the order of 0.5%. In the specific example shown in Fig. 1, the average DoLP value for the vehicle was measured to be 9%, while the overall average DoLP value of the natural background was measured to be 0.7%, which was driven primarily by the steep slope (orientation) of the terrain.

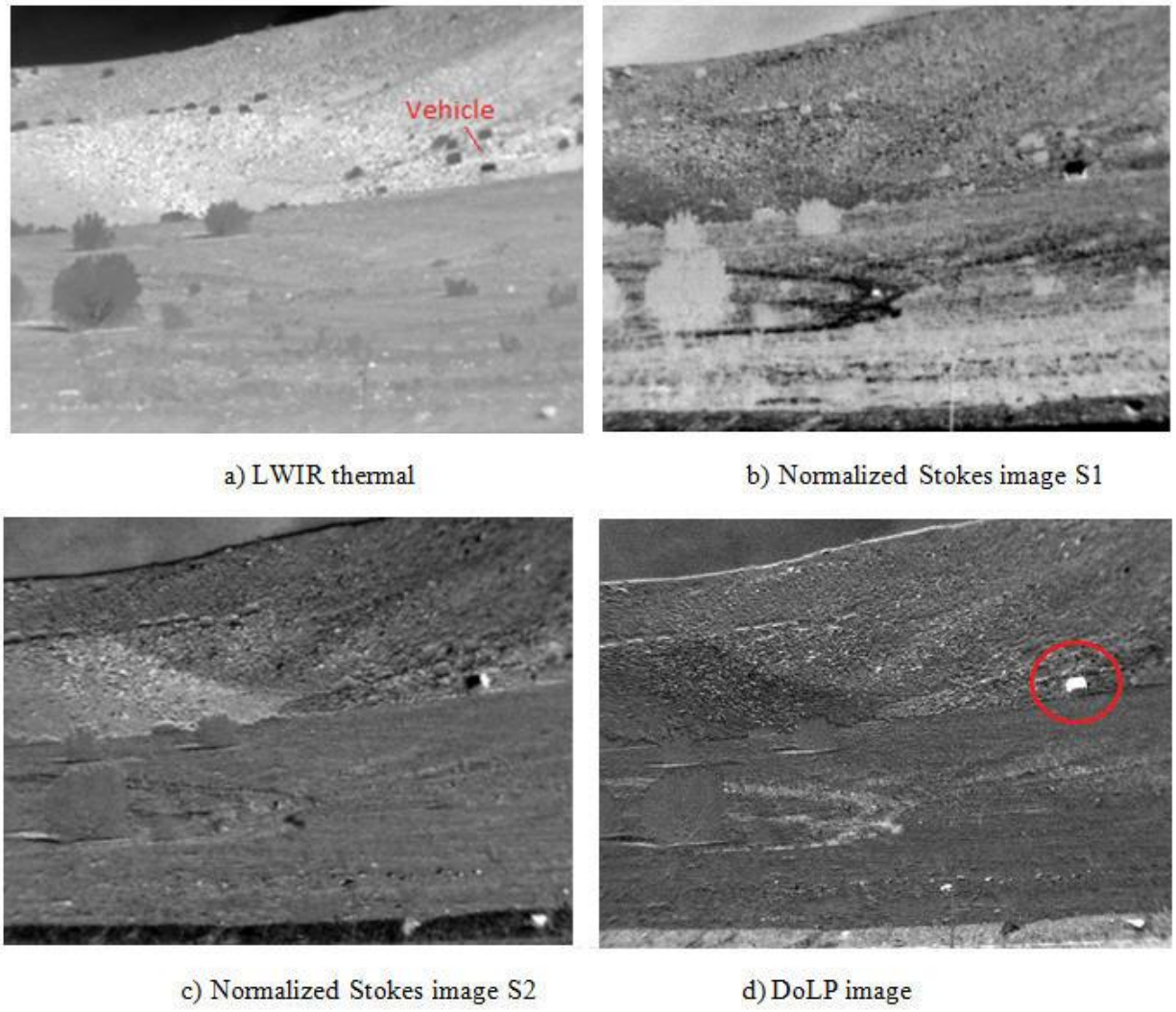

Fig. 1 Photographs are a typical polarimetric image set showing a vehicle parked against a natural background: a) shows a conventional LWIR thermal image S0, (w/sr-cm^2); b) and c) show the normalized Stokes images S1 and S2, respectively; and d) shows the DoLP image in which the silhouette of vehicle is clearly visible (highlighted circle).

2. Polarimetric Sensor

There are a variety of optical configurations appropriate for polarimetric imaging, e.g., division of amplitude (DoA), division of focal plane (DoFP), and division of aperture (DoAP).[4–6, 14, 15] However, for this study we chose to use a sensor based on a division-of-time (DoT) approach that relies on a spinning-achromatic-retarder (SAR) configuration to polarimetrically filter the LWIR radiance. Because the SAR method relies on the capture and differentiation of sequentially recorded images, it is most appropriate for imaging objects that are slowly moving or static within the scene. Although somewhat limited by the sequential nature of operation, the

SAR method is by far the best choice for research applications since it offers optimum radiometric throughput, spatial resolution, and excellent polarimetric sensitivity.

Figure 2a shows the basic design of a LWIR SAR-based imaging polarimeter that uses either a room-temperature microbolometer sensor or a cryogenically cooled Mercury Cadmium Telluride (MCT) focal-plane-array (FPA) detector for image capture. In general, we have found the MCT-based systems perform better than the microbolometer systems. Typical MCT-based FPAs tend to exhibit a noise-equivalent DoLP or NEDoLP (similar to NEΔT parameter often used to describe conventional thermal-imaging systems) on the order of ±0.1%, whereas the microbolometer-based systems exhibit NEDoLP values in the range of ±0.3–0.5%.

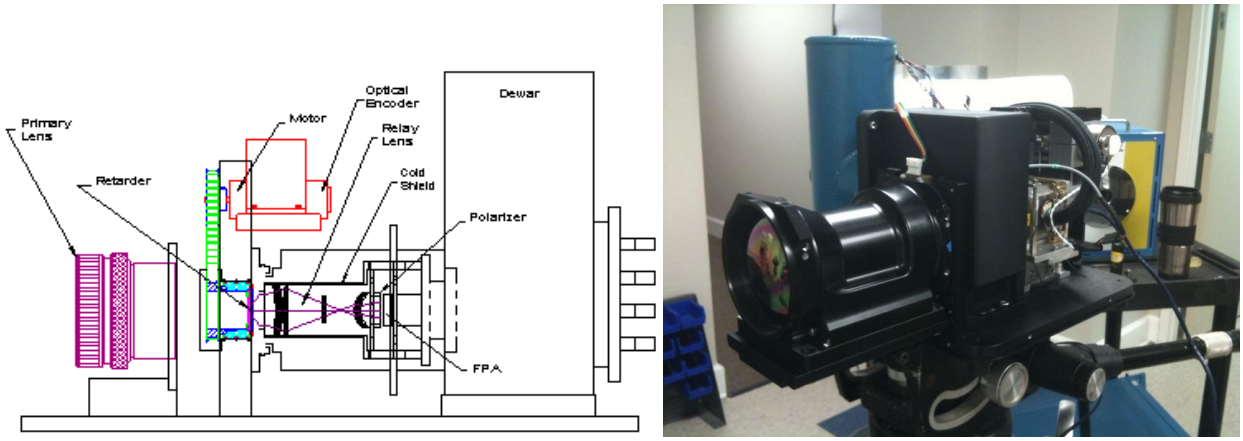

a) b)

Fig. 2 a) Typical optical configuration of the SAR design for the b) LWIR radiometric/polarimetric camera system

The particular LWIR polarimetric camera used for this study was a SAR sensor developed by Polaris Sensor Technologies, Inc., which uses a 640 × 480 MCT FPA that is cooled to liquid-nitrogen temperatures using a Sterling cooler. In the design shown in Fig. 2, the objective lens forms an image on an "intermediate" image plane just after the achromatic rotating retarder. The relay lens system translates the intermediate image onto the FPA, which is shielded from spurious radiance by a well-positioned cold stop. The achromatic retarder is located at a position in the optical train where all of the rays are paraxial, which allows for an extremely low pixel-misregistration error of less than 0.1 pixel.

As previously mentioned, the SAR imaging polarimeter performs a sequential measurement in time, where each image in the series is recorded at different orientation angles of the achromatic retarder. In its principle mode of operation, the system acquires a set of 16 images per rotation of the retarder. The polarizer is a custom wire-grid polarizer manufactured by Optometrics, Inc., that displays an extinction ratio in excess of 300:1 over the 7.5–11.1 μm sensitivity range of the FPA. The achromatic retarder is a custom cadmium sulfide/cadmium selenide (CdS/CdSe) wave plate fabricated by Gooch and Housego Inc. Finally, the front-end objective for the polarimetric

camera consisted of a dual-focal-length f/2 lens (i.e., 45 mm and 135 mm) produced by Ophir Optics, LLC.

3. Material Samples

Figure 3 has photographs of 3 samples described as "heat-shielding" materials consisting of an aluminum-foil backing that is coated with a white polymer binder.

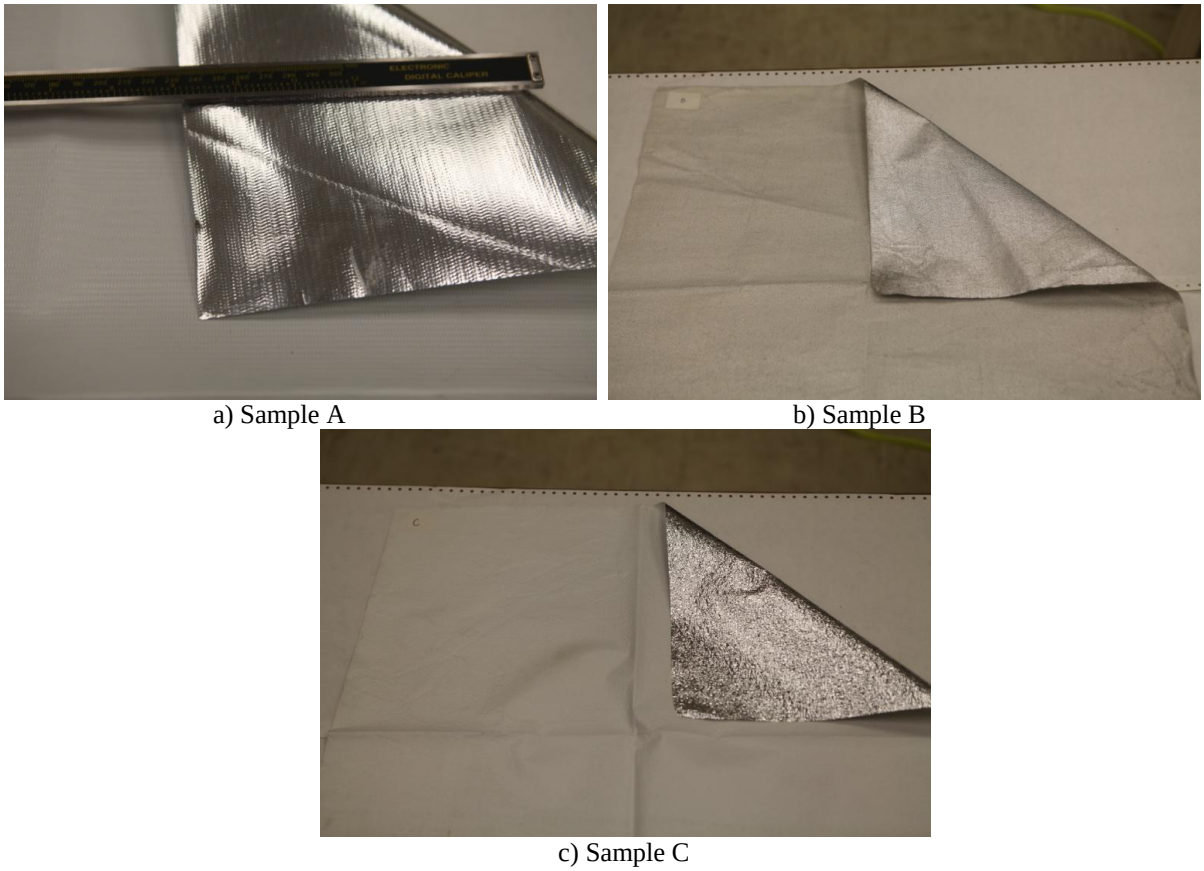

a) Sample A b) Sample B

c) Sample C

Fig. 3 Three aluminum-coated polymer samples of heat-shielding materials: Sample A is an aluminum-coated polymer exhibiting a fine grid pattern on both the aluminum and polymer sides; Sample B is described as an air-permeable material with a finely woven texture; and Sample C displays a "fine crinkled" pattern on the aluminum side.

The main distinguishing feature among the heat-shielding samples is the overall thickness of the aluminum-and-polymer binder and the texture/roughness of both sides. Sample A was by far the thickest material and had a relatively smooth finish on the white polymer, while Sample B was an air-permeable "cloth like" textile that was the most delicate in texture among the 3 heat-shielding samples. Sample C exhibited "fine crinkle" type finish on the aluminum side, while the white polymer side was relatively smooth.

The next category of samples considered was a series of nickel-coated Kevlar produced by Fiber Materials, Inc. These 2 materials, shown in Fig. 4a and 4b and identified as Samples D and E, were very similar except that the weave in Sample D appeared slightly tighter than in Sample E. Both materials were identified by the manufacturer as having the same nickel-content value of 115 g/m^2.

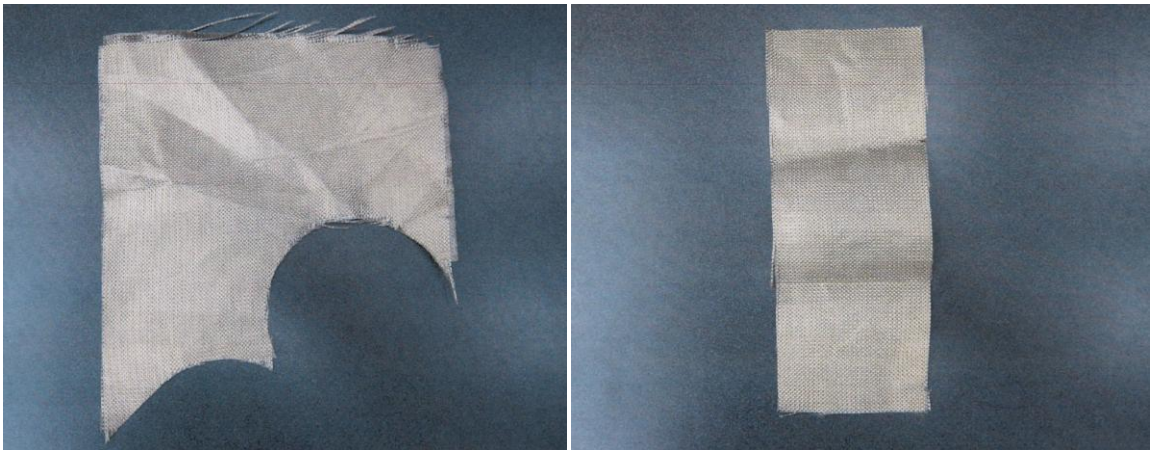

a) Sample D b) Sample E

Fig. 4 Photographs a) and b) show swaths of a nickel-Kevlar woven fabric with slightly different weave patterns, i.e., Sample D's weave pattern was slightly coarser than Sample E's. Both materials were reported to have a nickel content of 115 g/m^2.

The third category of textiles examined was a select series of electromagnetic interference (EMI) shielding fabrics labeled Samples F and G and shown in Fig. 5a and 5b. These EMI-suppressing materials were produced by International Paper Co., in its product line termed "SAF-N-60". The SAF-N-60 series was produced by weaving together fine strands of a silver-coated-polyester fiber into a fine fabric mesh that is best described as having the tactile feel of fine cotton.

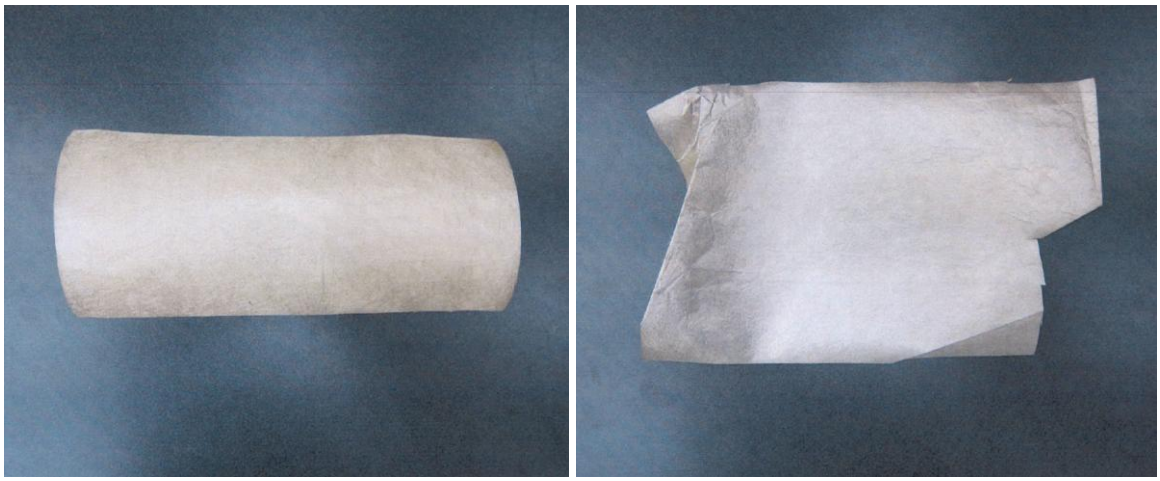

a) Sample F b) Sample G

Fig. 5 Samples F and G are silver-based EMI shielding materials consisting of a very finely woven mesh of a silver-coated-polyester fiber

Finally, Samples H and I, shown in Fig. 6a and 6b, are 2 carbon-based EMI materials produced by International Paper as part of its Carbon NanoWeave and Nickel Graphite NanoWeave product lines, respectively.

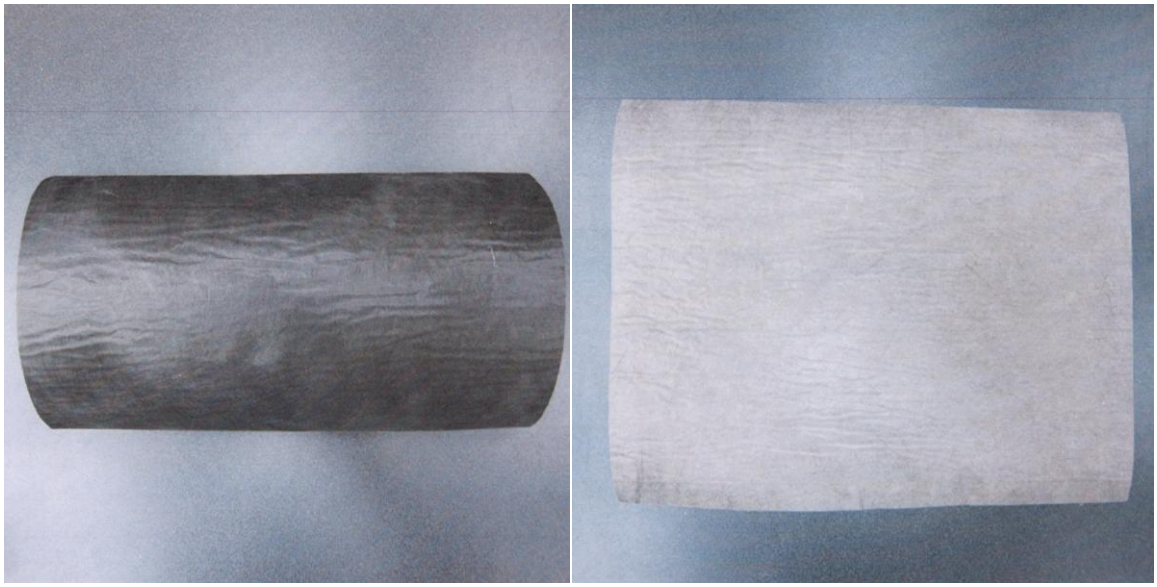

a) Sample H b) Sample I

Fig. 6 Two carbon-based EMI products of International Paper: Sample H is a uncoated Carbon NanoWeave material and Sample I is a Nickel Graphite NanoWeave textile

4. Measurement

Passive LWIR polarimetric and radiometric data were recorded over the 5-day period of May 13–17, 2013, at the US Army Research Laboratory in Adelphi, MD. The measurements were conducted outside where a electrically heated test panel and material samples were positioned 11.6 m from the polarimetric SAR camera (see Fig. 7a and 7b). Meteorological conditions were relatively cloud free and sunny for the 5 days with ambient temperatures ranging from a low of 22 °C (typical morning temperatures) to a high of 34–36 °C during late afternoon.

a) b)

Fig. 7 a) In the polarimetric-measurement setup the LWIR polarimetric camera is located in the shadow on the left side of the photograph. b) The heated test panel has 4 sample materials attached; a calibrated black body—van with camouflage netting—is positioned in the scene and is set at a constant temperature of 37 °C. Typical test-panel temperatures ranged from 40 to 50 °C depending on the degree of solar loading.

Because the heated test panel was exposed to varying degrees of solar loading, surface temperatures of the panel were monitored and recorded in order to correct for any extreme variation. During a typical morning-to-afternoon test session we noted that the panel temperature could change by as much as 10 °C from morning to afternoon, i.e., the average temperature ranged from 40 to 50 °C.

As reported in prior studies, we have found that ambient "cloud-based" radiance in the LWIR (and to a greater degree in the MidIR) can meaningfully affect polarimetric signatures for objects that are at moderate or ambient temperatures.[16–18] However, because no such cloud cover was experienced during our testing period, no appreciable variation in polarimetric response due to ambient effects were seen.

Each day during the testing period the polarimetric sensor underwent a series of radiometric and polarimetric calibrations runs by flood filling the front aperture with known radiance values via a calibrated black body. After the calibration was performed, samples were magnetically attached to the heated panel and allowed to reach thermal equilibrium. A series of 120 frames were recorded and averaged (approximately 2 s) for a particular sample set and panel-orientation angle. The resultant image set containing S0, S1, S2, and DoLP images are then digitally stored for later analysis.

A key aspect highlighting the additional information in a polarimetric image can be seen by comparing the 2 photographs in Fig. 8a and 8b. Figure 8 shows a typical set of resultant imagery used for analysis of 2 carbon-based materials, Samples H and I. Figure 8a shows a calibrated conventional LWIR thermal image whose pixel values are in units of (w/sr-cm^2). Figure 8b shows the same image except the degree of linear polarization is presented, where pixel values are displayed using a false color pallet to highlight the differences in the DoLP exhibited by both textiles. As shown in Fig. 8a, the apparent temperature difference (ΔT) between the sample

materials and the heated panel is small, and as a result exhibits poor contrast between the material surfaces and the panel. In this example the measured average radiance values for the right and left material samples were found to be 0.0036 and 0.0034 w/sr-cm² respectively, while the measured radiance for the heated panel was 0.0039 w/sr-cm². However, similar analysis for the polarimetric image shown in Fig. 8b identified DoLP values for the left and right sample as 5.1% and 1.3% respectively, while the heated-panel exhibited a DoLP value of 9.1%.

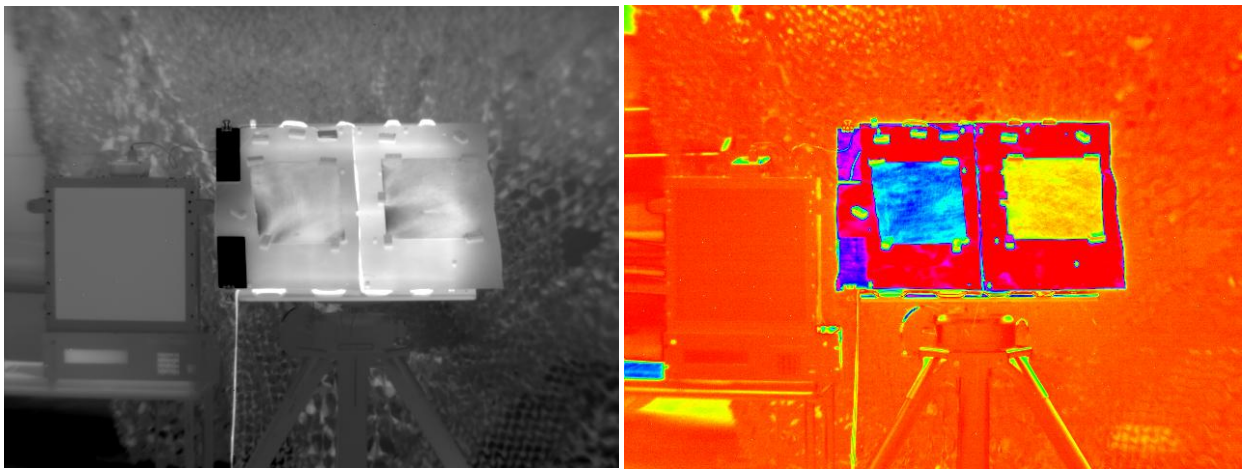

a) b)

Fig. 8 A typical raw image set used in the analysis: a) an LWIR thermal image, S0, of the 2 carbon-based materials, Samples H and I, which appear similar, and b) a resultant DoLP image defined by Eq. 4, showing quite different appearances when the polarization state is taken into account.

This simple example demonstrates the utility for considering the use of thermal polarimetric imaging in targeting, tracking, and identifying objects in various DOD-related applications. In practice, when objects of interest are in approximate thermal equilibrium with their surroundings, thermal contrast can be greatly reduced. However, when polarization information is extracted from the same thermal image, subtle differences in polarization state for the same scene can result in strong contrast between the target and background, even when ΔT is zero.

5. Results

The results of this study are presented in terms of radiometric- and polarimetric-response quantities. Since suppression of thermal emission by a particular material is independent of surface orientation, all radiometric quantities are derived from S0 images in which the heated mounting panel is fixed in the plane perpendicular to the line of sight (LOS), i.e., 0 degrees. Figure 9a–9d show the measured radiance values (w/sr-cm^2) emitted for defined regions of interest (ROI) recorded for each textile swatch. Also shown in Fig. 9a–9d are radiance values recorded from the unshielded portion of the mounting panel that surrounds each material. The difference in radiance values between the shielded and unshielded regions are shown in Fig. 9a–9d in the bar graph labeled DIFF.

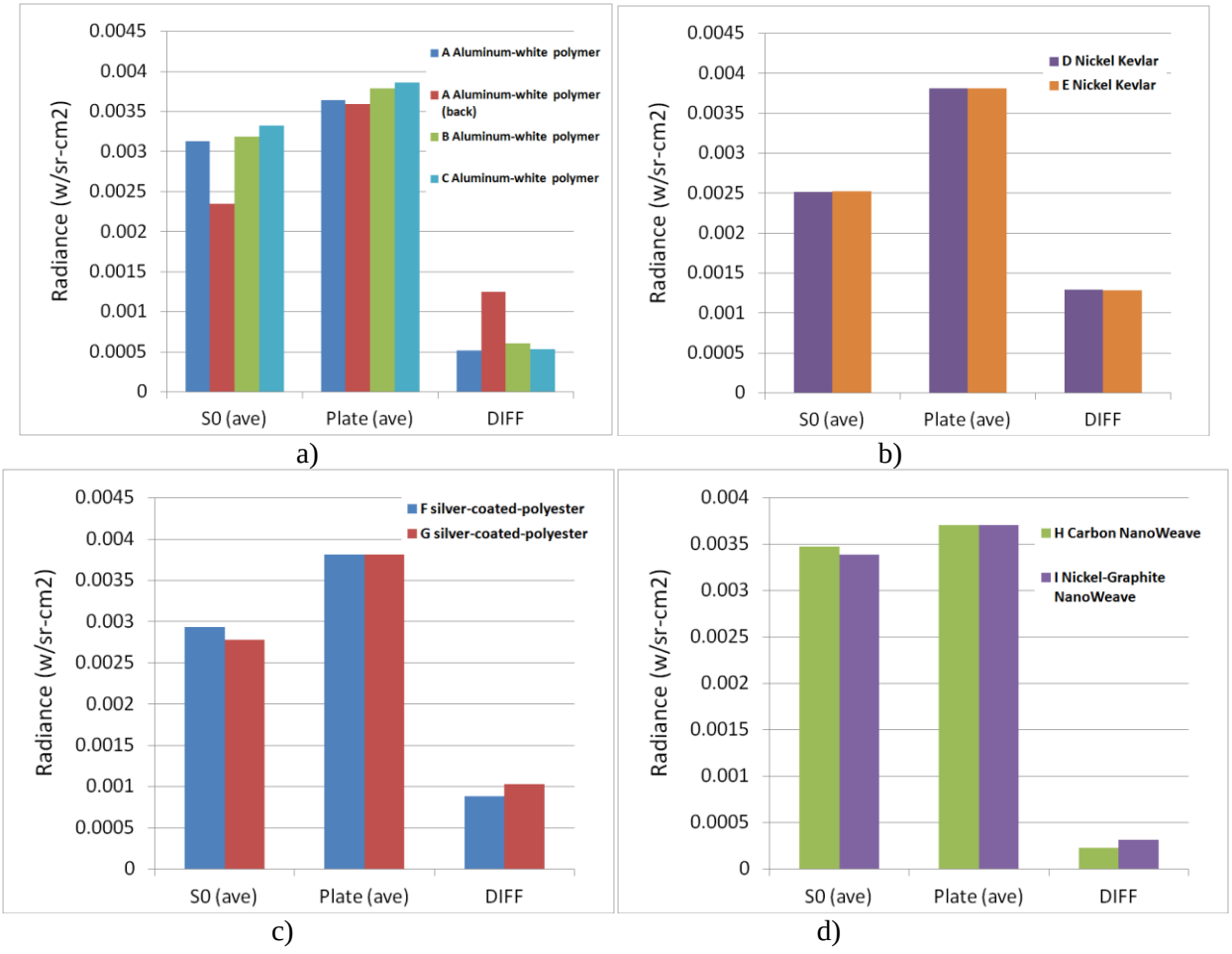

Fig. 9 Four parts show the measured radiance S0 (w/sr-cm^2) emitted from the surfaces of mounted swatches of materials as well as the unshielded mounting panel; also, each figure shows the recorded difference between the 2 surface regions.

Figure 10 shows a compilation of a simple thermal-suppression parameter, which is defined as the percentage of the overall radiance suppressed by each material. As shown, the nickel-coated Kevlar, in Samples D and E, suppressed the largest fraction of the overall radiance with a value of 34%, while the carbon-based textiles, Samples H and I, were the least effective, suppressing only 7–9% of the overall radiance.

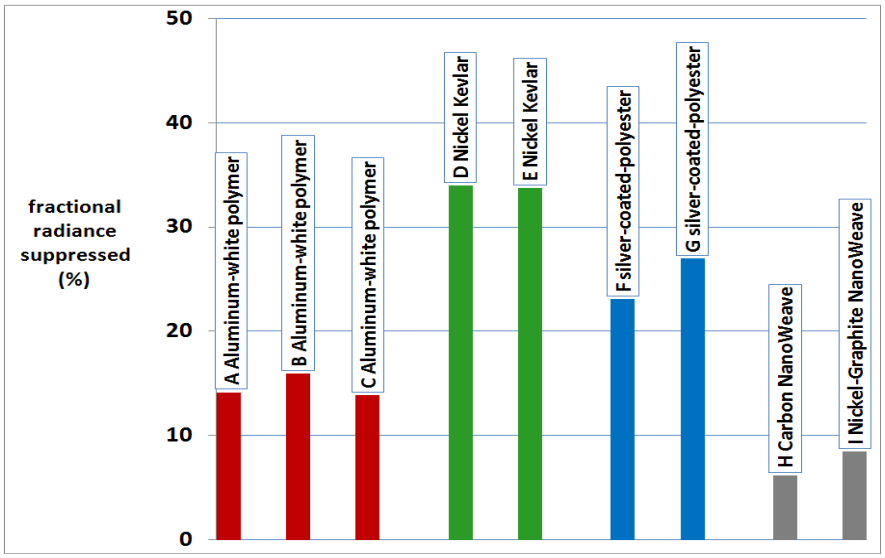

Fig. 10 Shows the fraction of the net radiance suppressed by each material

For the polarimetric portion of the study, we measured the Stokes images (S1, S2, and the resultant DoLP) as a function of surface orientation, which is defined as the angle between the surface normal and the LOS. (See Fig. 11–13.)

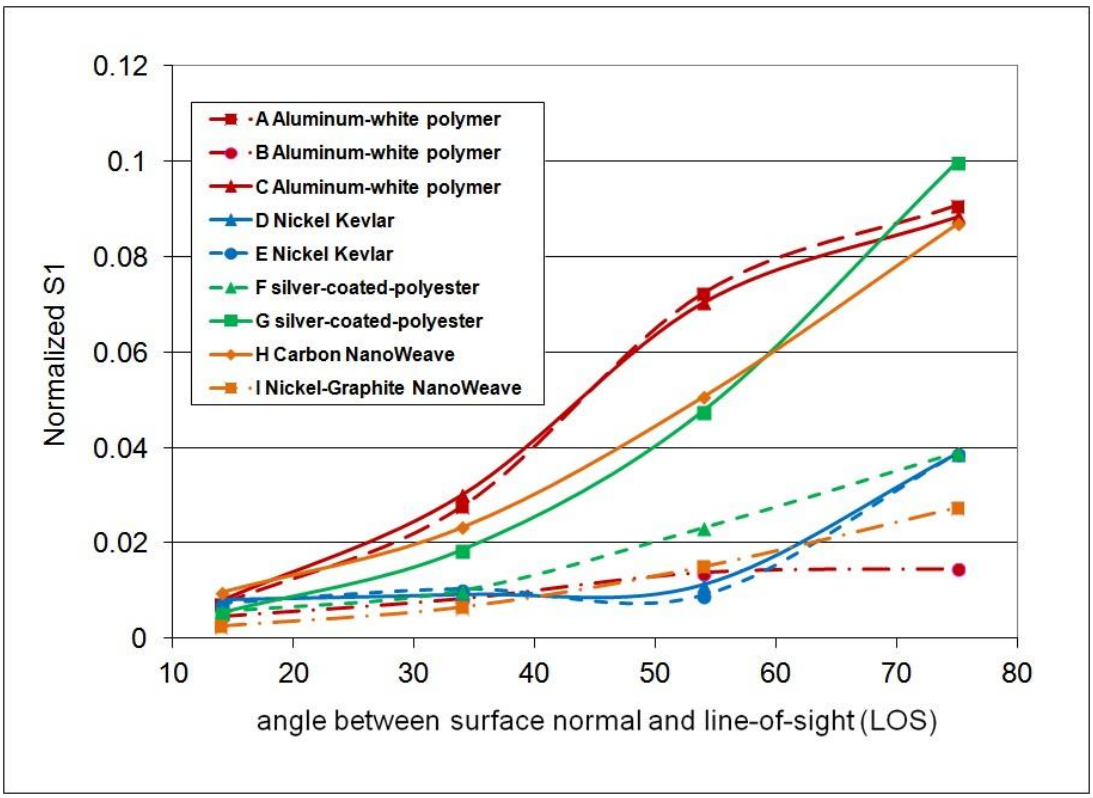

Fig. 11 Plots of the normalized S1 parameter as a function of surface orientation for the aluminum and white-polymer materials (red), the nickel-coated Kevlar (blue), the silver-coated polyester (green), and the carbon-based NanoWeave materials (orange)

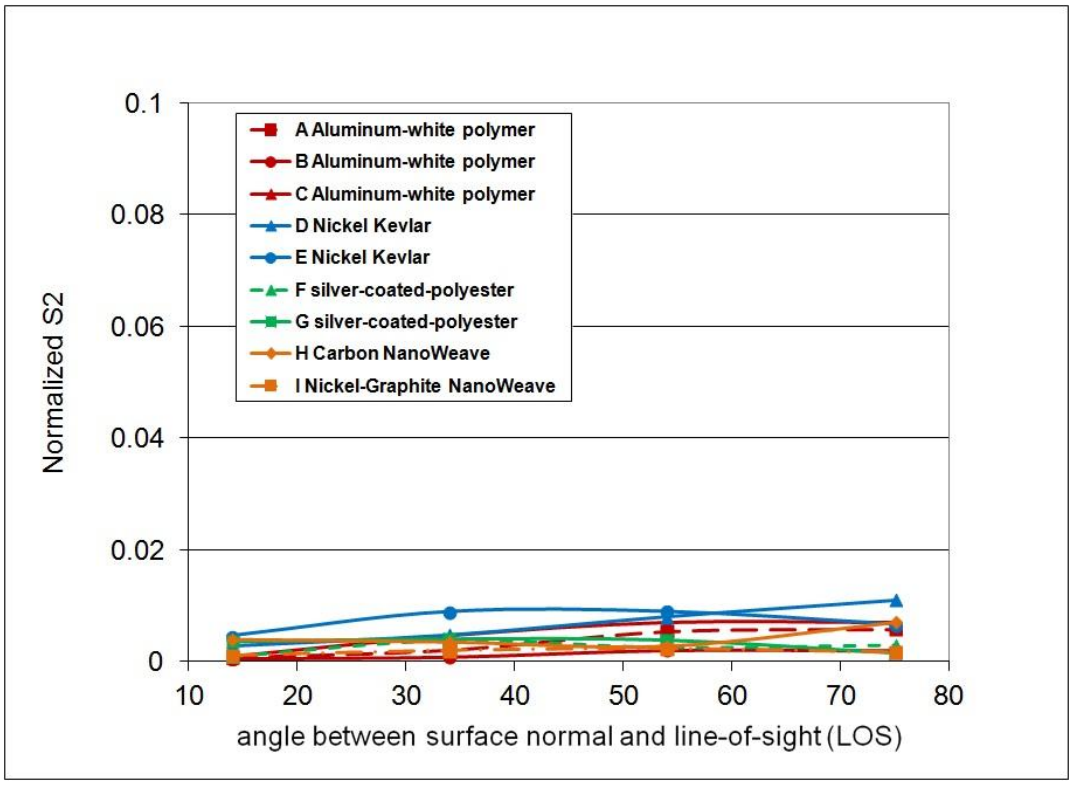

Fig. 12 Plots of the normalized S2 parameter as a function of surface orientation for the aluminum and white-polymer materials (red), the nickel-coated Kevlar (blue), the silver-coated polyester (green), and the carbon-based NanoWeave materials (orange)

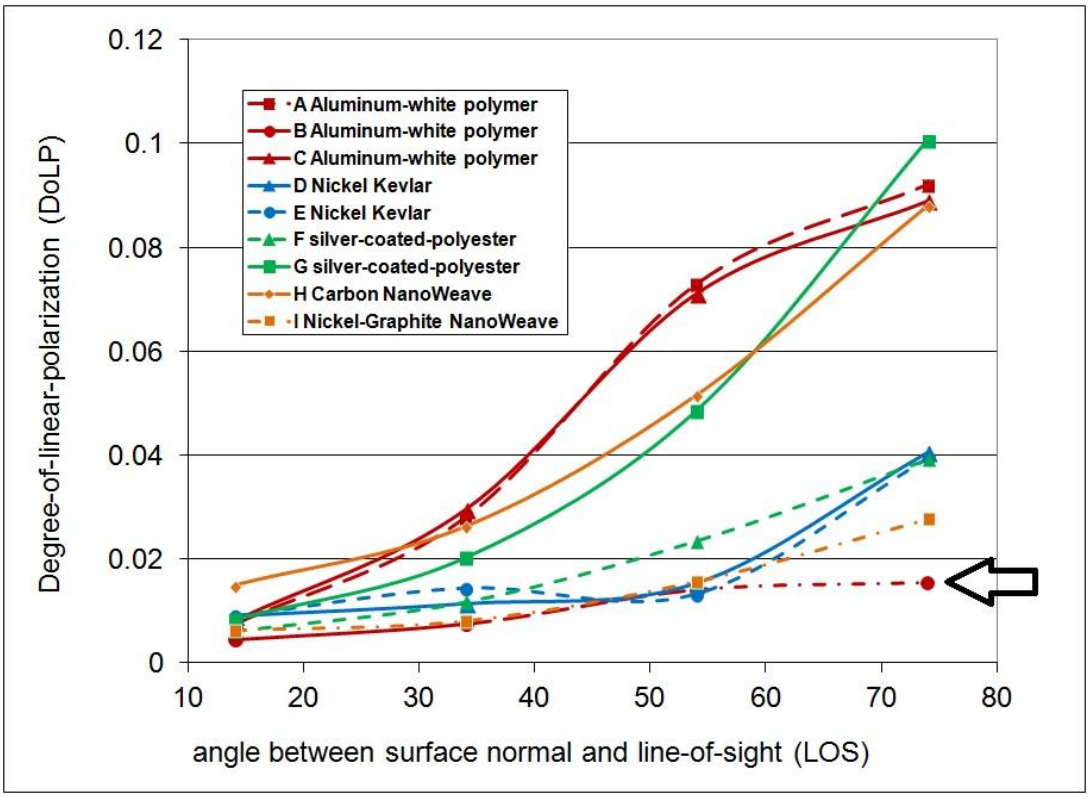

Fig. 13 Plots of the DoLP parameter as a function of surface orientation for the aluminum and white-polymer materials (red), the nickel-coated Kevlar (blue), the silver-coated polyester (green), and the carbon-based NanoWeave materials (orange). Black arrow points to an interesting response of Sample B (aluminum and white polymer): the polarized emission is greatly reduced due to destructive effects from surface-facet dimensions becoming comparable to the wavelength of emission.

In general, polarization that results from emission only (as opposed to reflection) is driven by 2 material characteristics: angle of orientation and surface roughness. Because the angle of incidence resides in a single plane for our measurement, only the S1 parameter resulted in any appreciable signal. As a result, the magnitude of the overall DoLP shown in Fig. 13 was driven primarily by S1 only. Examination of Fig. 11 shows the expected increase of linear polarization that is induced as the angle between the surface normal and LOS increases.

However, it is apparent that the grouping of materials into particular categories (e.g., Al-white-polymer, Ni-Kevlar, etc.), for the radiometric portion of the study has less significance since important polarimetric factors such as surface roughness and emissivity could vary significantly within a given group. A good example of this is seen by comparing the normalized S1 values (at large orientation angles) among the different samples of the aluminum-white polymer group shown in Fig. 11 and 13. Please note for this set of materials the white-polymer side (not the aluminum side) was the surface measured by the polarimetric sensor.

Although difficult to see in the photographs shown in Fig. 3a–3c, close examination of Samples A and C show that the 2 materials are actually a laminated composite fabric, which is produced

by bonding separate thin sheets of various materials together. Close examination shows that Sample A was a tri-layer composite material with a fabric center (polyester) that was sandwiched between a thin white layer of vinyl and a layer of aluminum. Similarly, Sample C was shown to be a bi-layer composite fabric in which 2 thin sheets of vinyl and aluminum are combined without the fabric center. In addition, the white vinyl laminate for Samples A and C had slightly different surface patterns engraved into the white polymer, yet the overall surface-roughness profiles were very similar due to the way the laminates were formed. This similarity in over-roughness gave rise to the nearly identical polarimetric response that is shown in Fig. 11–13 for Samples A and C.

Perhaps the most interesting material of the 9 textiles examined was Sample B. Even though grouped in the same category as Samples A and C, the composition of Sample B was quite different. Unlike the laminate structure seen in Samples A and C, Sample B consisted of a white-polyester woven fabric in which a thin layer of aluminum was sputtered onto 1 side of the fabric. As result, Sample B was the lightest in mass density and was the only sample that was air permeable. This allowed the material to retain a finely diffused pattern in which the weave of the closely knit fabric was still apparent. Close examination of the weave showed surface-facet dimensions (dimensions of the material weave) to be on the order of 0.1 mm or 100 μm. Since the wavelength of emission that is measured by the SAR polarimetric camera is on the order of 10μm, the ratio of emission wavelength to surface-facet dimension is on the order of 1/10. It has been reported that such conditions give rise to maximum attenuation of both reflected and meson-induced polarization resulting in the extremely low polarimetric response shown for Sample B in Fig. 11 and 13.[19, 20]

Examination of Fig. 11 and 13 shows that Samples G and H also exhibit good polarimetric response as demonstrated by normalized S1 and DoLP values greater than 8% for large orientation angles.

These 2 materials highlight the importance that surface geometry plays, rather than the bulk optical or electrical properties, in producing polarized thermal emission. Both materials were produced by International Paper's Advanced Fiber Nanowoven Group but consist of completely different bulk materials. Sample G consists of a silver-coated polyester that is characterized as having a low emissivity value and being a good electrical conductor, whereas Sample H is a carbon-based NanoWeave that is characterized as having a high emissivity value but is moderately conductive (see Fig. 5b and 6a). Although being quite different from a composition standpoint, the 2 samples exhibit a very similar geometry that is best described as a "tight-fine" weave structure, resulting is a "sheen" characteristic that is often associated with surfaces that are relatively smooth. It is the similarity in geometric shape of the 2 weaves that gives rise to nearly identical polarimetric responses (shown in Fig. 11 and 13) rather than optical/electrical properties.

The remaining samples, D, E, F, and I, were all coarsely woven silver- or nickel-coated textiles. We use the subjective term "coarsely" in the sense that the weave patterns for these materials are noticeably larger in dimension, e.g., 0.5–1.0 mm, compared to the fine weave patterns seen in samples B, H, and G. These weave patterns produce a much more diffuse surface which in turn gives rise to a lower polarimetric response of less than 4% for both normalized S1 and DoLP values (as shown in Fig. 11 and 13).

6. Conclusions

We examined the radiometric and polarimetric responses for a variety of textile materials that were categorized as either heat- or EMI-shielding materials. Specifically, we measured the intensity and polarization state of the thermal emission radiated from 9 sample materials that were mounted on a heated test panel that produced surface temperatures in the range of 40–50 °C. Radiometric and polarimetric quantities were measured as a function of surface orientation using a research-grade, SAR polarimetric camera that was sensitive in the IR-waveband region of 7.5–11.1 μm.

The primary radiometric quantity of interest was a measure of how effective each textile was in suppressing the overall heat flux produced by the panel. Results showed that the Kevlar-based materials were most effective in suppressing thermal signature by reducing the overall radiance by nearly 35% (see Fig. 10). We found it interesting that the aluminum and white-polymer laminates, Samples A, B, and C, that were produced explicitly for heat-shielding applications yielded a suppression fraction of 14–15% (see Fig. 10). One possible reason: Because the materials consisted of a nonpermeable, continuous matrix of plastic and aluminum (as opposed to the woven nature of the other samples), the laminates allowed a more efficient path for the conduction of heat.

In addition to the radiometric portion of the measurement, the polarization states of the thermal emission for the 9 samples were also examined. The Stokes images, S0, S1, S2, and the DoLP image were measured for the 9 samples under conditions of low, ambient atmospheric loading in the LWIR, i.e., clear sky.

In general, most of the materials behaved, from a polarimetric viewpoint, as expected; where the fabrics that exhibited large surface-roughness features displayed low degrees of linear polarization, while the "smooth" materials like the aluminum-polymer laminates showed an ever-increasing degree of linear polarization as the angle between the surface normal and LOS grew larger.

The 1 material that exhibited an unusually low degree of linear polarization was the aluminum-white polymer, Sample B, shown in Fig. 3b. Several studies involving surface-roughness effects on polarization emission describe a condition for reduced emission polarization that occurs when

the dimensions of certain surface-roughness features become “comparable” to the emission wavelength; for this study, the approximate emission wavelength was taken to be 10 μm. However, the exact conditions for optimum polarization suppression are still not well defined.[19, 20] Although somewhat anecdotal, we believe the response demonstrated by Sample B may shed some light on what might be considered an “optimum” surface condition for polarization suppression. As mentioned earlier, we concluded that the relevant roughness-facet dimension displayed in Sample B was on the order of 10λ. We concluded that it was this condition that resulted in an unusually low DoLP value of less than 2%, even at the largest surface-grazing angles. It is our hope to conduct future polarimetric studies to confirm these findings and improve our understanding of how to produce novel/new materials that are capable of better shielding the polarimetric signatures that have been demonstrated to be particularly strong for various man-made objects.

7. References

1. Sandus O. A review of emission polarization. Appl Opt. 1965;4:1634–1642.
2. Walraven R. Polarization Imagery. Opt Eng. 1981;20:14–18.
3. Wolfe J, Chipman RA. High-speed imaging polarimeter. In: Polarization Science and Remote Sensing, Shaw JA, Tyo JS, editors Proceedings of SPIE; 2003;5158:24–32.
4. Tyo JS, Goldstein D, Chenault D, Shaw J. Review of passive polarimetry for remote sensing applications. Appl Opt. 2006;45(22):5453–5469.
5. Kudenov M, Pezzaniti L, Gerhart G. Microbolometer-infrared imaging Stokes polarimeter. Optical Eng. 2009;48(6).
6. Pezzaniti JL, Chenault DB. A division of aperture MWIR imaging polarimeter. Proceedings of SPIE; 2005;5888,58880V.
7. Farlow CA, Chenault DB, Spradley KD, Gulley MG, Jones MW, Persons CM. Imaging polarimeter development and application. Proceedings of SPIE; 2001;4819:118–125.
8. Bowers D, Boger JK, Wellens LD, Black WT, Ortega SE, Ratliff BM, Fetrow MP, Hubbs JE, Tyo JS. Evaluation and display of polarimetric image data using long-wave cooled microgrid focal plane arrays. In: Proceedings of SPIE; 2006;6240:Polarization: Measurement, Analysis, and Remote Sensing VII.
9. Gurton KP, Felton M. Detection of disturbed earth using passive LWIR polarimetric imaging. Proceedings of SPIE Optics and Photonics Conference; 2009 Aug 2–6 San Diego (CA).
10. An C, Grantham J, King J, Robinson J, Pezzaniti L, Gurton K. Utility of polarization sensors for clutter rejection. 6th Annual US Missile Defense Conference; 2008 Mar 31–April 3; Washington (DC).
11. Gurton KP, Felton M. Detection of buried improvised explosive devices (IED) using passive long-wave infrared (LWIR) polarimetric imaging. Adelphi (MD): Army Research Laboratory (US); September 2009. Report No.: ARL-TR-4941.
12. Harchanko JS, Chenault DB, Farlow CF, Spradley K. Detecting a surface swimmer using long wave infrared imaging polarimetry. In: Photonics for Port and Harbor Security, DeWeert MJ, Saito TT, editors. Proceedings of SPIE; 2005;5780.
13. Hecht E, Zajac A. Optics. Reading (MA): Addison-Wesley Pub; 1979.

14. Chun CSL, Fleming DL, Torok EJ. Polarization-sensitive thermal imaging. In: Automatic Object Recognition IV, Sadjadi FA., editor. Proceedings of SPIE;1994;2234:275–286.

15. Pezzaniti JL, Chipman RA. Imaging polarimeters for optical metrology. In: Polarimetry: Radar, Infrared, Visible, Ultraviolet, and X-Ray, Chipman RA, Morris JW, editors. Proceedings of SPIE; 1990;1317:280–294.

16. Felton M, Gurton KP, Pezzaniti JL, Chenault DB, Roth LE. Measured comparison of the crossover periods for mid- and long-wave IR (MWIR and LWIR) polarimetric and conventional thermal imagery. Opt Exp. 2010;18(15):15704–15713.

17. Felton M, Gurton KP, Roth LE, Pezzaniti JL, Chenault DB. Measured comparison of the inversion periods for polarimetric and conventional thermal long-wave IR (LWIR) imagery. Proceedings of SPIE Optics and Photonics Conference, San Diego (CA), 2009 Aug 2–6.

18. Gurton KP, Felton M. Variation in MidIR and LWIR polarimetric imagery due to diurnal and metrological impact. In: Polarization: Measurement, Analysis, and Remote Sensing VIII, Proceedings of SPIE; Orlando (FL); 2008 Mar 17–19.

19. Jordan DL, Lewis G. Measurements of the effect of surface roughness on the polarization state of thermally emitted radiation. Opt Lett. 1994;19(10):692–694.

20. Gurton KP, Dahmani R, Videen G. Reduced polarized thermal emission due to surface contamination by dew and atmospheric aerosols. J Quan Spect Rad Tran. 2004;(88):61–70.

8. List of Symbols, Abbreviations, and Acronyms

CdS/CdSe	cadmium sulfide/cadmium selenide
DoA	division of amplitude
DoAP	division of aperture
DOD	Department of Defense
DoFP	division of focal plane
DoLP	degree of linear polarization
DoT	division of time
EM	electromagnetic
EMI	electromagnetic interference
FPA	focal-plane-array
IED	improvised explosive device
IR	infrared
LOS	line of sight
LWIR	long-wave infrared
MCT	Mercury Cadmium Telluride
MidIR	mid-wave infrared
NEDoLP	noise-equivalent degree of linear polarization
NIR	near-infrared
RDEC	Research, Development and Engineering Center
ROI	regions of interest
SAR	spinning achromatic retarder

1 (PDF)	DEFENSE TECH INFO CTR ATTN DTIC OCA (PDF)
2 (PDF)	US ARMY RSRCH LABORATORY ATTN IMAL HRA MAIL & RECORDS MGMT ATTN RDRL CIO LL TECHL LIB
1 (PDF)	US ARMY RSRCH LAB ATTN RDRL CIE S K GURTON
1 (PDF)	GOVT PRNTG OFC A MALHOTRA
1 (PDF)	NSRDEC NATICK, MA LISA HEPFINGER
1 (PDF)	NSRDEC NATICK, MA SCOTLUND MCINOSH

INTENTIONALLY LEFT BLANK.